

# Numerical and experimental study of moisture-induced stress and strain field developments in timber logs

Finn Larsen · Sigurdur Ormarsson

Received: 11 January 2012 / Published online: 24 April 2013  
© Springer-Verlag Berlin Heidelberg 2013

**Abstract** When solid wood dries from a green condition to a moisture content used for further processing, moisture-induced fracture and stresses can occur. The drying stresses arise because of internal deformation constraints that are strongly affected by the cross-sectional moisture gradient differential shrinkage and the inhomogeneity of the material. To obtain a better understanding of how stresses develop during climatic variations, the field histories of stresses (and strains) in cross sections in their entirety need to be studied. The present paper reports on experiments and numerical simulations concerned with analysing the development of strains and stresses during the drying of 15-mm-thick discs of Norway spruce timber log. The samples were dried at 23 °C and relative humidity of 64 % from a green condition to equilibrium moisture content. The moisture gradient in the longitudinal direction was minimised by use of thin discs simplifying the moisture history of the samples studied. The strain field history was measured throughout the drying process by use of a digital image correlation system. Numerical simulations of the samples agreed rather well with the experimental strain results obtained. The stress results also indicated where in the cross section and when fractures could be expected to occur during drying. More optimal drying schemes showed markedly reduced stress generation.

## Introduction

Solid wood is a hygroscopic, orthotropic and nonhomogeneous material, the stiffness properties of which are strongly affected by the moisture content (MC). The MC within a timber log in a green condition varies over the cross section, since the heartwood has a considerably lower initial MC than the sapwood. Solid timber

---

F. Larsen (✉) · S. Ormarsson  
Department of Civil Engineering, Technical University of Denmark, Brovej, 2800 Kgs. Lyngby,  
Denmark  
e-mail: finla@byg.dtu.dk

needs to be dried from a green condition down to moisture content below that of the fibre saturation point (FSP) before it can be used as a construction material. When a solid piece of timber contains both heartwood and sapwood, considerable stresses can develop during drying because of the large moisture gradients that arise. The heartwood part starts to shrink at an early stage since it reaches FSP much earlier than the sapwood part does. The drying history is likewise complex through drying occurring faster above than below the FSP. Experiments by Wiberg et al. (2000) and by Krabbenhøft (2003) on moisture loss above and below the FSP showed the rate of drying (evaporation) to be higher above the FSP than below it. It was found that above the FSP, the drying of wood is strongly dependent upon evaporation from the surface of the wood, and drying below the FSP was strongly dependent upon moisture transport inside the wood. Further numerical investigations of drying above the FSP were carried out by Salin (2006, 2010) who evaluated the occurrence of damage zones produced by sawing and by other actions affecting the wood surface as a function of the drying speed.

Mechano-sorptive strains that develop during the combined occurrence of moisture change and stress generation can reduce the occurrence of stresses related to drying. Numerous experiments have been conducted in efforts to identify mechano-sorption strains caused by changes in the ambient climate. Studies of the mechano-sorptive behaviour of wood material under constant loading and controlled climatic conditions were carried out by Armstrong and Kingston (1962), Lazarescu and Avramidis (2008) and Svensson (1995) who were able to identify and determine the magnitude of elastic, mechano-sorptive and visco-elastic strains. How mechano-sorption parameters affect the distortion of solid timber was investigated numerically by Ormarsson (1999) and Fortino et al. (2009), for example. Differences between shrinkage coefficients in the radial and the tangential directions were studied experimentally and were found to strongly affect the stress generation that occurs during the drying process (Dahlblom et al. 1999).

Moisture-related stress and strain fields in nonhomogeneous cross sections are extremely difficult to predict. Several numerical investigations taking different approaches to this were conducted: Felix and Morlier (1992) modelled stress and strain development in thin quadratic cross sections (discs). Clair et al. (2003) used discs taken from logs to investigate shrinkages properties, primarily in the radial and the tangential directions. Bonneau and Puiggali (1993) constructed a 2-zone model for analysing the drying of wood containing both heart and sapwood. Kang and Lee (2002) developed a mathematical model for studying strains and stress development (within a cross section) based on differences between MC in heartwood and in sapwood. The numerical results presented showed stress variations of interest within the cross sections. Later, Kang and Lee (2004) conducted an experimental investigation on radial shrinkage in solid wood discs. Kowalski and Smoczkiwicz-Wojciechowska (2007) made use of an acoustic emission method in experiments aimed at monitoring the state of stresses in dried wood discs. The experiments were performed such that evaporation could only occur from the bark of a cylindrical wood disc. Sreekanth and Kolar (2009) performed drying experiments at 130 °C in a specially constructed setting involving use of discs 30 mm in diameter for

studying crack propagation due to tangential stresses. The experimental findings were used to verify a model developed for predicting fracture behaviour.

The experiments reported in the present paper were conducted to examine strain field development during the drying of thin discs taken from a timber log. Since the drying of wood occurs much faster in the longitudinal direction than in any other directions, using thin discs enables the experimental time to be reduced appreciably and the moisture gradient in the longitudinal direction to be reduced to an absolute minimum. The degree of deformation constraint can also be varied by using discs with and without a slit from pith to bark, these having open and closed annual rings, respectively. The drying direction for kiln dried timber is predominant radial and tangential which is different from the direction in these experiments. The thin discs are used because they provide simple and well-defined moisture histories which facilitate calibration of the simulation model. The mechano-sorptive behaviour caused by moisture gradients (or internal constraint) during drying is universal regardless of the drying direction. The calibrated model is therefore useful in general and can easily be used for simulation of stresses and fracture of kiln dried timber boards, especially when drying of boards with large moisture gradients in green condition is simulated. Note, large gradient can occur in wooden discs because they consist of both heartwood and sapwood with marked difference in green moisture content. The degree of variation in the transversal strain fields within the cross sections of the wood was measured during the drying process by means of a DIC system (Aramis 2007). The experimental samples were also simulated by use of a 3D distortion model developed by Ormarsson et al. (1998, 1999), the moisture content history and the shrinkage properties of the samples being obtained in the experimental study.

## Materials and methods

The research method employed is a combined experimental and numerical one. Strain fields in thin disc specimens obtained from a solid timber log were measured during drying by use of the DIC system, simulations of the drying stresses and strains being performed by use of a finite element model.

### Strain field measurements

#### *Test specimens*

The test specimens were selected from a timber log (1.5 m long and 200 mm in diameter) of a 20-year-old Norway spruce tree growing in the North Zealand section of Denmark and felled in January 2009. After the log was removed from the tree, it was cross cut into four sections before being placed in a freezer for conservation purposes. The disc-shaped specimens to be studied were later cut from the respective sections of the log in a frozen condition so as to avoid moisture loss during preparation of the specimens. The specimens were carefully selected (see Fig. 1) from areas as far as possible free of defects and with the aim of obtaining

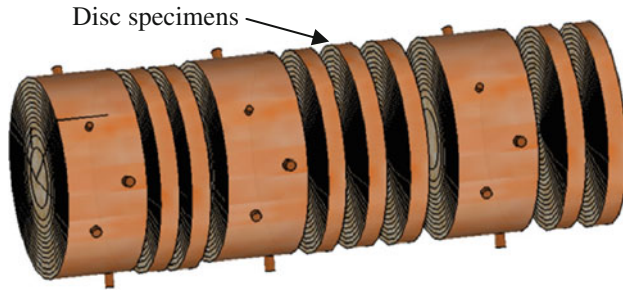


**Fig. 1** Principle of selecting test specimens

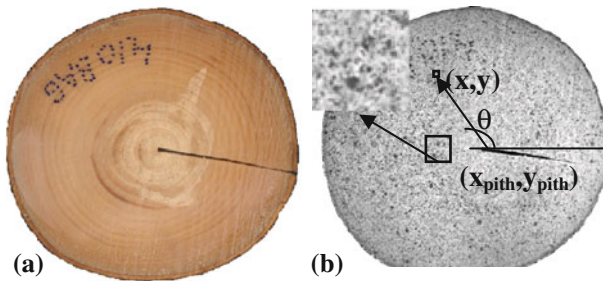


**Fig. 2** **a** Disc specimen with a slit, **b** sprayed specimen with random pattern used for Aramis measurements

samples as homogeneous (in tangential direction) as possible so as to keep the effects of variations in the material properties at a minimum. Even such carefully selected specimens varied to some extent, the colour variations are shown in Fig. 2, indicating there to be certain variations both in moisture content and in material properties.

To reduce internal constraints within the disc specimens during the drying process that followed, a 1.5-mm-wide slit was sawn from the bark to the pith; see Fig. 2a.

### Experimental setup

To study drying deformations of the specimen by use of the DIC system, the disc was placed on a stand containing a digital weight cell together with fan ventilation around the disc (see Fig. 3). An arbitrary pattern of dots, as shown in Fig. 2b, was sprayed on the surface for use in obtaining strain measurements. The entire strain field history of the disc specimen was measured by the DIC system; at the same time, the weight of the test specimen, together with the temperature and RH of the surrounding air, was recorded by a logger at 15-min intervals.

Both the temperature and the RH were kept constant throughout the experiments with values of  $23 \pm 1$  °C and  $63 \pm 2$  % RH. According to the Hailwood–Horrobin equation adapted for wood by Simpson (1973) and described in Baronas et al. (2001)

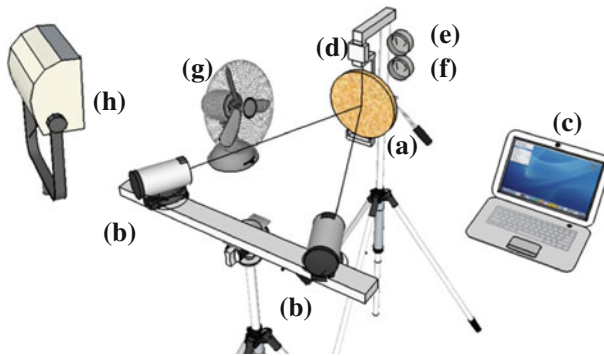


**Fig. 3** Experimental setup: **a** disc specimen, **b** digital cameras, **c** computer for data logging, **d** weight cell, **e** relative humidity gauge, **f** temperature gauge, **g** fan ventilation, **h** cold light

and Ball et al. (2001), the EMC of the samples could be expected to reach about 12 %. For a more detailed description of the experimental setup, see Larsen et al. (2011). The dry weight of the specimens was determined by oven drying at 103 °C.

### Data recording

The strain field across the surface of the disc was measured by the DIC system. The system recognised the surface pattern of the specimen on the basis of digital images, coordinates being assigned to the pixels of the images. Initial images obtained in the undeformed stage served as the reference state, the image stages thereafter being recorded during the deformation phase of the specimen with the use of fixed intervals. The DIC system computes displacements and strains occurring from one image to another by means of movements of small square facets that are typically  $15 \times 15$  pixels in size with a  $2 \times 15$  pixel area of overlap with each neighbouring facet. The normal strains ( $\varepsilon_x$  and  $\varepsilon_y$ ) and shear strains ( $\gamma_{xy} = 2\varepsilon_{xy}$ ) are found for each of the facets. The principal strains, termed major and minor strains ( $\varepsilon_1$  and  $\varepsilon_2$ ), which are based on the two types of strains just referred to, are calculated by use of Eq. (1). Note that the minor strains can be numerically the largest if these are negative or if both the major and the minor strains are negative. The angle between the x-axis and the first principal axis (1-axis) is also calculated by use of the DIC system on the basis of Eq. (2).

$$\varepsilon_{1,2} = \frac{\varepsilon_x + \varepsilon_y}{2} \pm \sqrt{\left(\frac{\varepsilon_x + \varepsilon_y}{2}\right)^2 + \varepsilon_{xy}^2} \quad (1)$$

$$\varphi = 0.5 \tan\left(\frac{2 \cdot \varepsilon_{xy}}{\varepsilon_x - \varepsilon_y}\right)^{-1} \quad (2)$$

### Further processing of the experimental data

To compare the strains measured by use of DIC system with simulated strains, those strains referring to the (x, y) coordinate system were transformed to the

coordinate system  $(r, t)$  of the wood material. The disc specimens studied had almost circular annual rings, and the pith was located close to the centre of the discs. Each facet in the undeformed state has  $(x, y)$  coordinates in the DIC system. The values for all other facets were estimated on the basis of the coordinates for the facets covering the pith and the radial and tangential directions, making use of the angle between the  $x$ -axis and the radius, the latter extending from the pith to the facet; see Fig. 2b.

The strain transformation from the  $(x, y)$  coordinate system to the  $(r, t)$  coordinate system is given in matrix form as

$$\bar{\varepsilon} = G\varepsilon \quad (3)$$

or

$$\begin{bmatrix} \varepsilon_r \\ \varepsilon_t \\ \gamma_{rt} \end{bmatrix} = \begin{bmatrix} \cos^2 \theta & \sin^2 \theta & \sin \theta \cos \theta \\ \sin^2 \theta & \cos^2 \theta & -\sin \theta \cos \theta \\ -2 \sin \theta \cos \theta & 2 \sin \theta \cos \theta & \cos^2 \theta - \sin^2 \theta \end{bmatrix} \begin{bmatrix} \varepsilon_x \\ \varepsilon_y \\ \gamma_{xy} \end{bmatrix} \quad (4)$$

where  $\bar{\varepsilon}$  represents the transformed strains in the directions  $(r, t)$  of the wood material,  $G$  is the transformation matrix, and  $\varepsilon$  contains the measured strains in the global coordinate system  $(x, y)$ .

## Modelling

Simulation of the disc specimens that were studied was performed by the finite element (FE) software Abaqus (2008), a 3D stress analysis being carried out using 8-node linear brick elements of type C3D8. The type of specimen studied was a circular 15-mm-thick disc divided into 20 geometrical parts, consisting of a small pith area and 19 annual rings. These parts were connected by a so-called tie-constraint that allowed the disc to function as an inhomogeneous continuum. Each part of it has its own set of material parameters and its own moisture and temperature histories. The simulation model involved the use of special routines for wood distortion developed by Ormarsson (1999). The model takes account of elastic deformation, moisture-induced shrinkage and mechano-sorptive deformation. Visco-elastic deformations are not taken account of, since according to investigations conducted by Svensson (1997), drying-related visco-elastic strains represent only a very small part of the total strains. The references employed concerned a local coordinate system including the  $l$  (longitudinal),  $r$  (radial) and  $t$  (tangential) directions, the pith serving as the centre. The experimentally observed changes in moisture content beneath the FSP functioned as a driver for the deformations. The initial variations in MC (under the green conditions,  $t = 0$ ) as well as the development of the MC curve over time were obtained along the radius ( $r$ ) of the discs. Figure 4 shows the result of the measured moisture history for the disc specimen used to provide input data for the model. In the model, the moisture content field over the cross section is assumed to be axisymmetrically distributed around the pith.

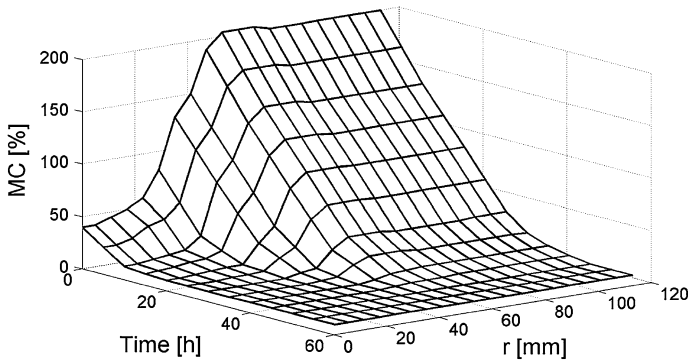


**Fig. 4** MC history used as input for simulation of the disc specimen

## Results and discussions

The development of the strain field over the cross section of the disc specimen was measured during drying, the results being used to verify the simulation model. The strain results at various times (obtained from the DIC system and FE software) were compared, although here the results for just one time level (25 h of drying) will be presented.

### Experimental verification of the simulation model

#### Material parameters

Table 1 shows the material parameters used in the simulation model. Both the parameters and the indices refer to notations described in Ormarsson (1999). The stiffness, mechano-sorptive, shrinkage and temperature parameters used are representative parameters for Norway spruce trees.

A typical expression for the modulus of elasticity and its rate of change as functions of MC and temperature are given by

$$E_i = E_{i0}(1 + E_{iT}(T_0 - T)) + E_{iw}(w_{f0}(1 + w_{fT}(T_0 - T)) - w_a) \quad (5)$$

$$\dot{E}_i = E_{iw}(-w_{f0}w_{fT}\dot{T} - \dot{w}_a) - E_{i0}E_{iT}\dot{T} \quad (6)$$

where the index  $i$  represents the material directions ( $l$ ,  $r$ ,  $t$ ),  $E_{i0}$  is the basic elastic modulus, and  $G_{i0}$  is the basic shear modulus, both of them at the reference temperature  $T_0 = 20$  °C,  $E_{iT}$ ,  $E_{iw}$ ,  $G_{iT}$  and  $G_{iw}$  representing the effects of the temperature and of the moisture level on the reference modulus. The additional parameters contained in the Table are Poisson's ratios  $\nu_{ij}$ ; the mechano-sorption behaviour  $m_{i0}$ ,  $m_{iT}$ ,  $m_{iw}$ ; the coefficients  $\mu_{ij}$  describing the coupling between the mechano-sorption effect in the different directions; the shrinkage coefficients  $\alpha_i$ ; the coefficients  $w_{f0}$ ,  $w_{fT}$  representing the fibre saturation point; the reference temperature  $T_0$ ; and the initial temperature  $T$ . The difference between the radial shrinkage coefficients for heartwood and for sapwood was obtained in an experimental study presented in

**Table 1** Material parameters used in the simulations

$E_{l0} = 9,700 \text{ MPa}$	$E_{r0} = 400 \text{ MPa}$	$E_{t0} = 220 \text{ MPa}$
$E_{lT} = 0.013 \text{ }^\circ\text{C}^{-1}$	$E_{rT} = 0.013 \text{ }^\circ\text{C}^{-1}$	$E_{tT} = 0.013 \text{ }^\circ\text{C}^{-1}$
$E_{lw} = 21,000 \text{ MPa}$	$E_{rw} = 2200 \text{ MPa}$	$E_{tw} = 1,300 \text{ MPa}$
$\nu_{lr} = 0.35$	$\nu_{lt} = 0.60$	$\nu_{rt} = 0.55$
$G_{lr0} = 400 \text{ MPa}$	$G_{lt0} = 250 \text{ MPa}$	$G_{rt0} = 25 \text{ MPa}$
$G_{lT} = 0.013 \text{ }^\circ\text{C}^{-1}$	$G_{lT} = 0.013 \text{ }^\circ\text{C}^{-1}$	$G_{rT} = 0.013 \text{ }^\circ\text{C}^{-1}$
$G_{lrw} = 1,163 \text{ MPa}$	$G_{ltw} = 122 \text{ MPa}$	$G_{rtw} = 72 \text{ MPa}$
$m_{l0} = 0.0001 \text{ MPa}^{-1}$	$m_{r0} = 0.15 \text{ MPa}^{-1}$	$m_{t0} = 0.2 \text{ MPa}^{-1}$
$m_{lT} = -0.01 \text{ }^\circ\text{C}^{-1}$	$m_{rT} = -0.01 \text{ }^\circ\text{C}^{-1}$	$m_{tT} = -0.01 \text{ }^\circ\text{C}^{-1}$
$m_{lrT} = -0.01 \text{ }^\circ\text{C}^{-1}$	$m_{ltT} = -0.01 \text{ }^\circ\text{C}^{-1}$	$m_{rtT} = -0.01 \text{ }^\circ\text{C}^{-1}$
$m_{lrw} = 0.008 \text{ MPa}^{-1}$	$m_{ltw} = 0.008 \text{ MPa}^{-1}$	$m_{rtw} = -0.8 \text{ MPa}^{-1}$
$\mu_{lr} = 0.0$	$\mu_{lt} = 0.0$	$\mu_{rt} = 1.0$
$\alpha_l = 0.0071$	$\alpha_{r\_heart} = 0.10$	$\alpha_{t\_heart} = 0.20$
$\alpha_{\text{slope}} = -0.038$	$\alpha_{r\_sap} = 0.17$	$\alpha_{t\_sap} = 0.35$
$T_0 = 20 \text{ }^\circ\text{C}$	$w_{j0} = 0.30$	$w_{jT} = 0.0033$
$T = 23 \text{ }^\circ\text{C}$	$w_{\text{init}} \geq 0.30$	$E_{l0\_slope} = 0.0$

Larsen et al. (2010, 2011). A similar difference has been confirmed by Rosner et al. (2009), for example. The tangential shrinkage coefficient ( $\alpha_t$ ) was assumed to be twice as large as the radial coefficient ( $\alpha_r$ ) both for heartwood and for sapwood. Note that both of the indices  $i$  and  $j$  represent the material directions ( $l$ ,  $r$ ,  $t$ ).

## Experimental results

For the disc specimens studied, development of the strain field was measured during the drying process by use of the DIC system, the slit opening next to the bark being measured at regular time intervals as well. The correlation between the experimental and simulated results was assessed for the strain state attained after 25-h drying. Figures 2b, 5 and 6 show the deformation state that resulted after 25 h of drying, and Fig. 4 shows the conditions present when the heartwood reached EMC of 12 %, the sapwood at that point still lying significantly above the FSP. Note that the slit shown in Fig. 2b, which originally was 1.5 mm wide, had closed in the sapwood area and become wider than 1.5 mm in the heartwood area. This occurred because of the tangential shrinkage of the heartwood material striving to open the slit, at the same time as the opening of it was suppressed by the sapwood, which had not yet started to shrink, while the radial shrinkage in the heartwood area dragged the sapwood towards the pith, resulting in the closing of the slit in the sapwood area.

Strain plots from the DIC system show that minor strains, which all were negative and the numerically largest strains represented the limiting values. In most areas, the directions of the strains were nearly tangential, this corresponding closely to the direction of the largest shrinkage coefficient. In the heartwood area, close to the free edges of the slit in particular, much larger strains occurred than in the remainder of the cross section. The minor plots from the DIC system were almost identical with the transformed strain plot shown in Fig. 5a.



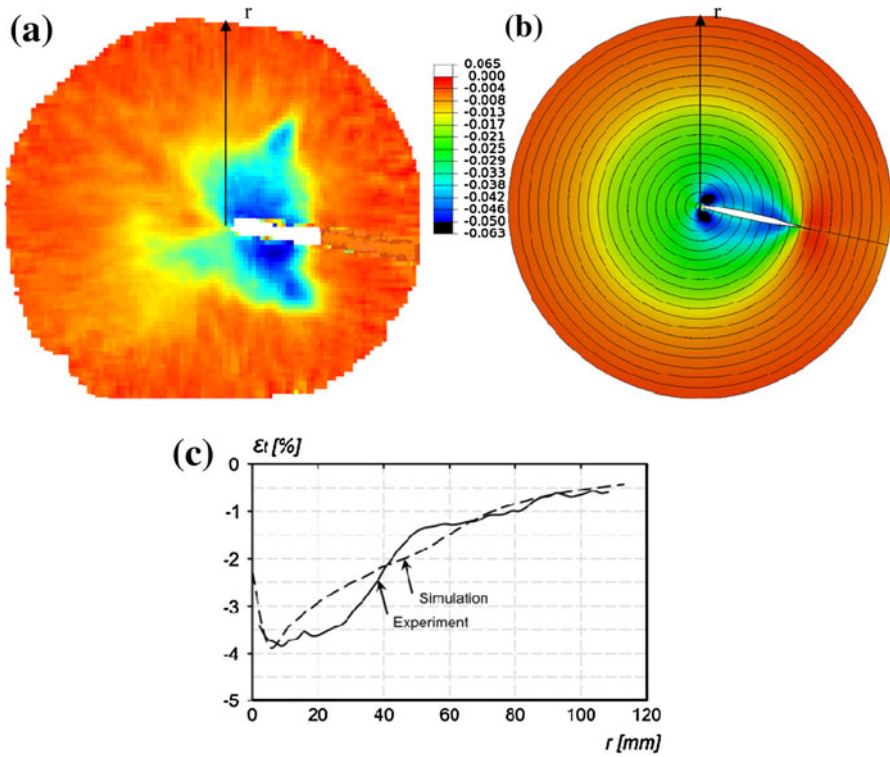


**Fig. 5** Tangential strain distribution after 25-h drying. **a** Measured strain, **b** simulated strain, **c** strain variation along the path  $r$

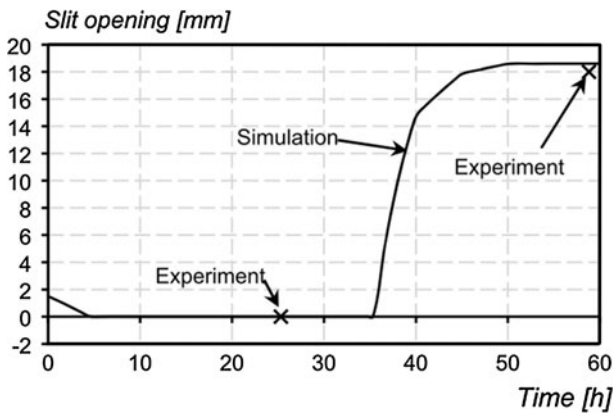


**Fig. 6** Variation in the slit opening during drying

## Verification of the simulation model

The global strains ( $\varepsilon_x$ ,  $\varepsilon_y$  and  $\varepsilon_{xy}$ ) that were measured by the DIC system were transformed into tangential and radial directions so as to be comparable to the simulated strains. Figure 5 shows the transformed tangential strains and the simulated strains at the same point in time. The simulated strain field in Fig. 5b shows tendencies similar to those of the transformed one shown in Fig. 5a, except for certain uneven strain variations. The path  $r$  used to compare experimental and numerical strains in terms of their variation is shown in Fig. 5a and b, the results obtained being shown in Fig. 5c.

The variations in strains along path  $r$  show an acceptable degree of correspondence between the experimental and the simulated result. The measured slit opening after 25 h of drying and at the final EMC stage corresponded rather closely in size to that of the simulated opening shown in Fig. 6. After the model was verified experimentally, it was used to investigate strain, stress and the development of distortion of the disc specimen during the drying process as a whole.

## Simulation results

### Strain development

To study in a more detailed way the moisture-related behaviour of the disc specimens, simulation results obtained along the path  $r$  were used to investigate how strains and stresses develop during drying. The tangential strains and stresses were studied because of the cracks propagating primarily from pith to bark due to tangential stresses exceeding the tensile strength of the material.

The simulation results presented in Fig. 7 indicate that strain development in one part of the disc (e.g. in the sapwood) is affected by the moisture history and the shrinkage behaviour in other parts and vice versa. For example, the central part (from the pith outward to a radius of 20 mm) showed material properties and a moisture history that in the case of free shrinking would have been identical

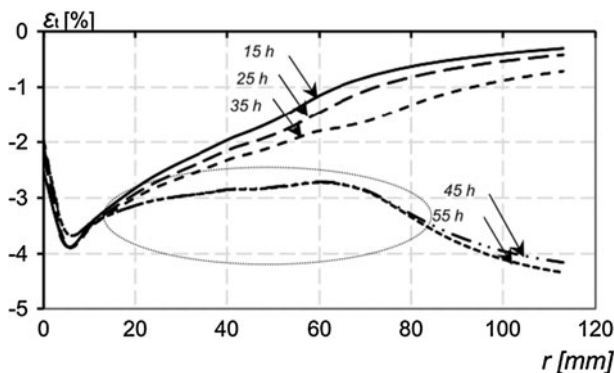


**Fig. 7** Variation in the (total) tangential strain development along  $r$  at different times during drying

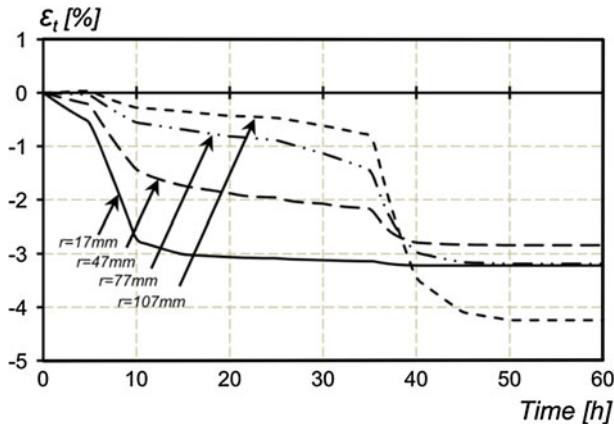


**Fig. 8** History plots for tangential strain located at different distances from the pith

throughout, although under the conditions present the surrounding material partly hindered shrinking, this generating stresses and mechano-sorption strains that led to a reduction in the total value of the tangential strains. The same phenomenon could be noted in the sapwood area. By comparison, the strain of free tangential shrinking was about 5 % after 45 h of drying. The marked curves in Fig. 7, which represent 45 and 55 h of drying, respectively, show marked mechano-sorptive strain behaviour. The sapwood closest to the bark was least affected by this mechano-sorptive behaviour. Figure 8 shows historical plots of the tangential strain at different positions along the path. Note the elastic strains in the sapwood area ( $r = 77$  and  $r = 107$  mm) during the first 35 h of drying before the sapwood area starts to shrink, and how the strains are largest close to the heartwood.

### *Stress development*

The mechano-sorption effects make the stress development difficult to predict. Figure 9 presents plots of the tangential stress along the path  $r$  at different drying times. Figure 10 shows historical plots of the tangential stress at fixed locations along the same path. Figure 9 indicates large variations in stress for all the drying times that were studied. The largest stress gradients occur close to the pith and within the transition zone between the heartwood and sapwood. The largest tensile stresses occur close to the pith at the end of the drying process. This is caused mainly by a local stress concentration that builds up in front of the tip of the slit when the slit starts to open. The tensile stresses within the transition zone are found to be very close in size to the tensile strength of the material. The sapwood begins shrinking after about 35 h of drying, as clearly evident in Figs. 8 and 10. Shortly after this, the slit starts to open (see Fig. 6), which changes the stress distribution markedly within cross section as a whole. The most pronounced changes occur in the transition zone between the heartwood and the sapwood (see curves  $r = 47$  mm and  $r = 77$  mm in Fig. 10). The stress generation in this zone is strongly affected by the early shrinking of the heartwood and the simultaneous resistance of the

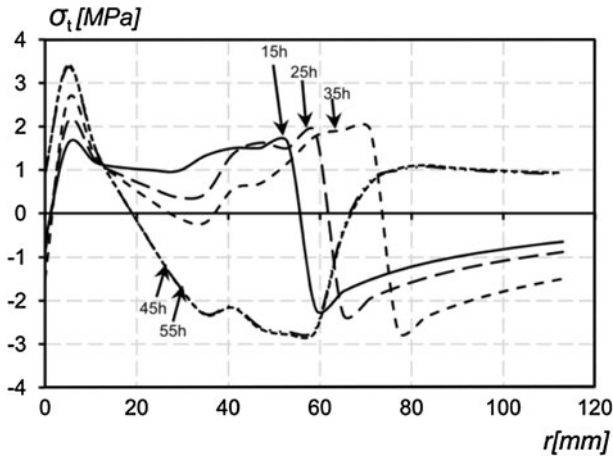


**Fig. 9** Variation in the tangential stress along  $r$  at different drying times

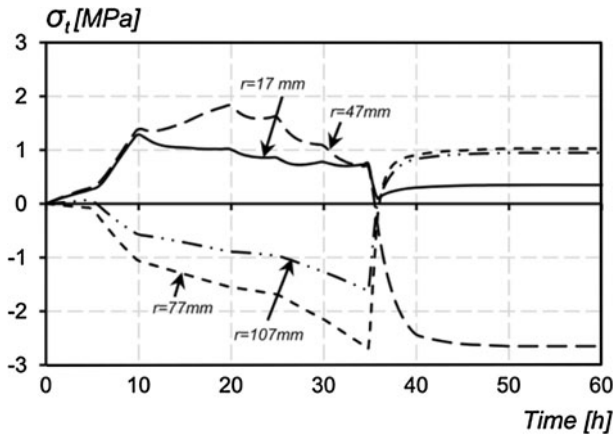


**Fig. 10** History plots for tangential stress located at different distances from the pith

sapwood, followed by shrinking of the sapwood and constraint caused by the heartwood when it has reached EMC. The largest compressive stresses occur in the middle zone at the end of the drying process, whereas the large tensile stresses in this zone occur much earlier in the drying process.

#### Effects of the drying schedules on the development of stress

Further numerical investigations were performed to examine how different drying conditions affect the development of strains and stresses. Instead of using constant climatic conditions as in the experimental study (63 % RH and 23 °C applying there), two variable drying schedules were employed. The first schedule began with

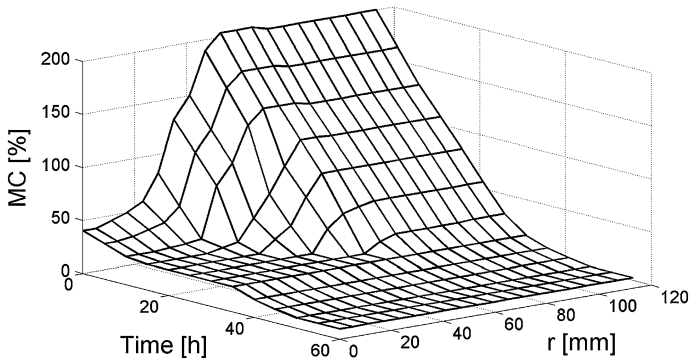


**Fig. 11** Moisture content history for the disc specimen, when the starting climate condition was 23 °C, 95 % RH and the ending condition was 23 °C, 63 % RH

a relative humidity of 95 % RH and a temperature of 23 °C, until all parts of the disc had reached EMC, which was  $EMC = 23\%$  according to the Hailwood–Horrobin equation. From this stage onward then, the moisture history based in the experimental results was followed down to where  $EMC = 12\%$ . In terms of the Hailwood–Horrobin equation,  $EMC = 23\%$  when conditions of 95 % RH and 23 °C are reached. The moisture history used as input for simulation of the disc specimens is presented in Fig. 11.

The second drying schedule began with climate conditions of 95 % RH and 60 °C, changes that occurred then leading, just like for the first schedule, to conditions of  $EMC = 12\%$ . Under these initial climate conditions, the equilibrium moisture content became  $EMC = 20\%$ . During this simulation, the temperature was held at 60 °C. These two schedules aimed at removing the free water from the sapwood, before the disc specimen as a whole was dried to lower moisture content, resulting in virtually no MC gradient below the FSP. Each of the three drying schedules lasted for 60 h and ended at  $EMC = 12\%$ . For each of the schedules beginning at 95 % RH, the course of MC from 40 to 60 h was the same.

Variations in stress along path  $r$ , as shown in Fig. 9, can be compared with those caused by each of the two modified moisture histories. Figure 12 shows the variations in tangential stresses caused by the three drying schedules after 15 and 45 h of drying.

Figure 12 shows substantial reductions in the stresses occurring under the conditions that the modified drying schedules involved. The stress reduction in the diagram for 15 h of drying was most evident for the schedule with the highest temperature, although at 95 % RH the EMC was lower at this temperature. These results indicate the clear effect of temperature on the elasticity and mechano-sorptive properties of the discs. Table 2 shows how the elastic moduli and mechano-sorption parameters change from 23 to 60 °C. Both the reduction in the elasticity modulus and the increase in the mechano-sorption parameters lead to an increase in mechano-sorptive strain and a reduction in constraints at 60 °C, this resulting in a lower stress level.

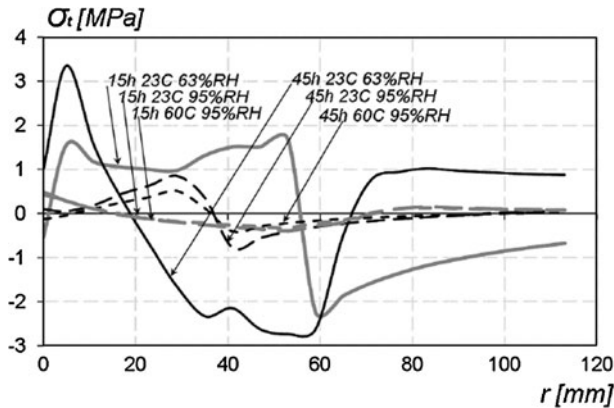


**Fig. 12** Influence of drying schemes on variation of tangential stress along the path  $r$  after 15- and 45-h drying

**Table 2** Stiffness and mechano-sorption parameters for different temperatures at EMC with 95 % RH

Temp. (°C)	Parameters
23	$E_t = 286 \text{ MPa}$
23	$E_r = 510 \text{ MPa}$
23	$m_t = 0.21 \text{ MPa}^{-1}$
23	$m_r = 0.16 \text{ MPa}^{-1}$
60	$E_t = 184 \text{ MPa}$
60	$E_r = 325 \text{ MPa}$
60	$m_t = 0.28 \text{ MPa}^{-1}$
60	$m_r = 0.21 \text{ MPa}^{-1}$

At the end of the drying process, there was almost no discernible difference between the stress values for the two modified drying schedules, despite their obvious differences in the level of variation in stresses earlier in the drying process.

## Conclusion

The results for the experimental strain field (as recorded by DIC system Aramis) for the disc specimen that was studied were used to verify the simulation model. The material parameters used in earlier model investigations of Norway spruce were found to be appropriate here. The model was used to simulate the distribution of moisture-related strains and stresses within the disc specimens, making use of moisture histories based on different drying schedules that were similar to schedules in practical use in kiln drying. The results of the simulations clearly emphasise the decided effect that drying schedules have on stress development during the drying process.

Drying schedules beginning at 95 % RH (slow drying at the start) showed more marked stress reductions than found under climate conditions of 63 % RH. The

modified drying schedules employed showed the final stress level not to be affected by the temperature level. Differences between the material properties of the heartwood and the sapwood were found to have only a limited effect on the stress development as compared with the much larger effects that variations in MC had.

### Future work

Further numerical results are to be verified by experiments to be conducted in a new climate chamber at DTU.byg, where strain developments are to be measured by use of Aramis under ambient climate conditions that correspond to those of typical kiln drying. A major aim of this work will be to enable drying schedules to be optimised more effectively through reducing the stresses that occur during drying, this in turn serving to reduce the risk of crack propagations. Another aim of the experiments that are planned will be to clarify the time consumption within different drying schedules so as to be able to better optimise the drying process through taking both time relations and stress developments in the wood into account.

**Acknowledgments** This study was funded by The Danish Forest and Nature Agency, Haraldsgade 51, 2100 København Ø.

### References

- Abaqus (2008) Theory manual v6.8. Simulia
- Aramis v6 User Manual (2007) GOM mbH, GOM Optical measuring techniques. ([www.gom.com](http://www.gom.com))
- Armstrong LD, Kingston RST (1962) The effect of moisture content changes on the deformation of wood under stress. *Aust J Appl Sci* 13:257–276
- Ball RD, Simpson IG, Pang S (2001) Measurement, modelling and prediction of equilibrium moisture content in *Pinus radiata* heartwood and sapwood. *Holz Roh-Werkst* 59:457–462
- Baronas R, Ivanauskas F, Juodeikienė I, Kajalavicius A (2001) Modelling of moisture movement in wood during outdoor storage. *Nonlinear Anal Model Control* 6(2):3–14
- Bonneau P, Puiggali J-R (1993) Influence of heartwood-sapwood proportions on the drying kinetics of a board. *Wood Sci Technol* 28:67–85
- Clair B, Jaouen G, Beauchêne J, Fournier M (2003) Mapping radial, tangential and longitudinal shrinkages and relation to tension wood in discs of the tropical tree *Symphonia globulifera*. *Holzforschung* 57:665–671
- Dahlblom O, Petersson H, Ormarsson S (1999) Characterization of shrinkage, European project FAIR CT 96-1915, Improved spruce timber utilization, final REPORT Sub-task AB1.5
- Felix S, Morlier P (1992) Modelling of stresses and strains in a piece of wood under drying. *Holzforschung* 46:369–377
- Fortino S, Mirianon F, Toratti T (2009) A 3D moisture-stress FEM analysis for time dependent problems in timber structures. *Mech Time-Depend Mater* 13:333–356
- Kang W, Lee N-H (2002) Mathematical modelling to predict drying deformation and stress due to differential shrinkage within a tree disk. *Wood Sci Technol* 36:463–476
- Kang W, Lee N-H (2004) Relationship between radial variations in shrinkage and drying defects of tree disks. *J Wood Sci* 50:209–216
- Kowalski SJ, Smoczkiewicz-Wojciechowska A (2007) Stresses in dried wood. Modelling and experimental identification. *Transp Porous Med* 66:145–158
- Krabbenhöft K (2003) Chapter 4 and 5, Moisture transport in wood. A study of physical-mathematical models and their numerical implementation. Ph.D. Thesis. ISBN nr. 87-7877-225-7. Denmark
- Larsen F, Ormarsson S, Olesen JF (2010) In: Proceedings of the 11th international IUFRO wood drying conference, 2010, Luleå University of Technology, Skellefteå, Sweden, pp 137–144

- Larsen F, Ormarsson S, Olesen JF (2011) Moisture-driven fracture in solid wood. *Wood Mater Sci Eng* 6(1–2):49–57
- Lazarescu C, Avramidis S (2008) Drying related strain development in restrained wood. *Dry Technol* 26(5):544–551
- Ormarsson S (1999) Numerical analysis of moisture-related distortions in sawn timber. PhD thesis. ISBN 91-7197-834-8. Göteborg, Sweden
- Ormarsson S, Dahlblom O, Petersson H (1998) A numerical study of the shape stability of sawn timber subjected to moisture variation part 1: theory. *Wood Sci Technol* 32:325–334
- Ormarsson S, Dahlblom O, Petersson H (1999) A numerical study of the shape stability of sawn timber subjected to moisture variation part 2: simulation of drying board. *Wood Sci Technol* 33:407–423
- Rosner S, Karlsson B, Konnerth J, Hansmann C (2009) Shrinkage processes in standard-size Norway spruce wood specimens with different vulnerability to cavitation. *Tree Physiol* 29:1419–1431
- Salin J-G (2006) Modelling of the behaviour of free water in sapwood during drying. *Wood Mater Sci Eng* 1:4–11
- Salin J-G (2010) Problems and solutions in wood drying modelling: history and future. *Wood Mater Sci Eng* 5:123–134
- Simpson WT (1973) Predicting equilibrium moisture content of wood by mathematical models. *Wood Fiber Sci* 5:41–49
- Sreekanth M, Kolar AK (2009) Transient thermal behavior and stress development within a cylindrical wooden disk during drying in a fluidized bed dryer. *Dry Technol* 27:344–358
- Svensson S (1995) Strain and shrinkage force in wood under kiln drying conditions. *Holzforschung* 49:363–368
- Svensson S (1997) Internal stress in wood caused by climate variations. Report TVBK-1013. Lund University
- Wiberg P, Sehlstedt-Persson SMB, More'n TJ (2000) Heat and mass transfer during sapwood drying above the fibre saturation point. *Dry Technol* 18(8):1647–1664